Characterisation of Mechanochemically Synthesised Alane (AlH$_3$) Nanoparticles

M. Paskevicius, D.A. Sheppard, C.E. Buckley*

Department of Imaging and Applied Physics, Curtin University of Technology, GPO Box U 1987, Perth, WA, Australia

Abstract

A mechanochemical synthesis process has been used to synthesise alane (AlH$_3$) nanoparticles. The alane is synthesised via a chemical reaction between lithium alanate (LiAlH$_4$) and aluminium chloride (AlCl$_3$) at room temperature within a ball mill and at 77 K within a cryogenic mill. The reaction product formed consists of alane nanoparticles embedded within a lithium chloride (LiCl) by-product phase. The LiCl is washed with a solvent resulting in alane nanoparticles which are separated from the by-product phase but are kinetically stabilised by an amorphous particle surface layer. The synthesis of a particular alane structural phase is largely dependent on the milling conditions and two major phases (α, α') as well as two minor phases (β, γ) have been identified. Ball milling at room temperature can also provide enough energy to allow alane to release hydrogen gas and form aluminium metal nanoparticles. A comparison between XRD and hydrogen desorption results suggest a non-crystalline AlH$_3$ phase is present in the synthesised samples.

Keywords: Amorphous materials; Hydrogen storage materials; Nanostructures; Mechanochemical synthesis; X-ray diffraction

*Corresponding Author

C.E. Buckley

Department of Imaging and Applied Physics, Curtin University of Technology, GPO Box U 1987, Perth, WA, Australia

Email C.Buckley@curtin.edu.au

Phone 61 8 92663532

Fax 61 8 92662377

1. Introduction

Alane is a metal hydride with a high 10.1 wt.% gravimetric hydrogen capacity. It was first synthesised in a pure form in 1947 [1], but despite its usefulness in a number of industries it has not become widely available primarily due to difficulties in large-scale wet chemical synthesis [2]. Alane has potential applications in the fields of hydrogen storage, chemical catalysis, explosives, propellants and pyrotechnics. As such a number of recent studies have focussed on investigating AlH_3 structural and hydrogen sorption properties. Three of the AlH_3 crystal structures were only recently solved [3-5] even though they had been known to exist for over 30 years [6]. A number of studies have also been undertaken to investigate the kinetics of decomposition of AlH_3 [7, 8] including the effect of dopants and/or particle size on the kinetics [9, 10].

Traditionally bulk quantities of alane were primarily synthesised via a wet chemical process [6], however the formation of AlH_3 from its elements has also been undertaken under high hydrogen pressure (~2.5 GPa) [11, 12]. In the last few years certain novel experimental techniques have been used to synthesise AlH_3 including electrochemical charging [13], supercritical fluid hydrogenation [14], and a range of AlH_3 adducts have been formed which were found to be reversible under much milder hydrogen pressures [15]. The wet chemical process used for alane production involves the synthesis of an alane-ether complex within a solvent (usually diethyl ether) as follows [7]:

$$AlCl_3 + 3LiAlH_4 + n[(C_2H_5)_2O] \longrightarrow 4AlH_3 \bullet 1.2[(C_2H_5)_2O] + 3LiCl \qquad (1)$$
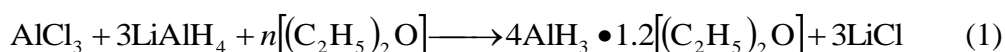
The wet chemical synthesis of AlH_3 is very sensitive to both temperature and time [7] and as such large-scale production and structural phase selection via this method is very difficult. There are seven structural phases (α, α', β, γ, δ, ε, ζ) which have been synthesised from the wet chemical method under various temperature, pressure and reaction conditions during the ether removal [6]. A mechanochemical synthesis method for alane has been performed previously in the literature [3] which involves the mechanical initiation of the following reaction:

$$\text{AlCl}_3 + 3\text{LiAlH}_4 \longrightarrow 4\text{AlH}_3 + 3\text{LiCl} \qquad \Delta_r G_{298K} = -191\,\text{kJ/mol}$$
$$\Delta_r G_{77K} = -158\,\text{kJ/mol}$$

$$(2)$$

The reaction progresses both at room temperature and at 77 K due to the relatively high change in Gibbs free energies. Brinks et al. [3] surmised that room temperature synthesis was inefficient in synthesising AlH_3 due to the low alane yields and high Al content. Aluminium forms due to the high milling energy at room temperature which allows for AlH_3 to decompose to Al and H_2. As a result, cryogenic milling is the preferred synthesis method in synthesising AlH_3 because low temperatures maintain lower milling temperatures, restricting AlH_3 decomposition. In the present work, room temperature milling was attempted under a variety of milling conditions (ball size, ball to powder ratio, and time) to explore its usefulness in the synthesis of a variety of alane structural phases and in minimising the aluminium content. Cryomilling at 77 K was also undertaken in order to provide a comparison of synthesis techniques, and a washing procedure was utilised to remove the salt by-product from the AlH_3 nanoparticles.

Mechanochemical synthesis differs from standard ball milling. A standard ball milling process results in a reduction in the particle size of a sample and eventually the formation of nanosized grains within micron-sized particles [16]. However the mechanochemical method involves the initiation of a solid-state displacement reaction during the ball milling process [16] which can result in nanosized particles (down to 4 nm in size [17]) embedded within larger by-product phase particles. Mechanical milling is utilised in the mechanochemical synthesis of nanoparticles because it effectively blends the reactants, forming nanoscale mixtures and increases the chemical reactivity (and also the reaction kinetics) leading to a chemical reaction between these reactants enabling the product phase to form [18]. The mechanochemical synthesis process has been used in the past [19, 20] to synthesise a broad range of metal nanoparticles as well as other compounds such as oxides and sulphides.

Particle size control can be gained by adjusting such factors as: the volume fraction of the by-product phase formed during milling, milling time, milling collision energy (ball-to-powder mass ratio and ball size) [18], milling temperature, and the use of process control agents [20]. The addition of a buffer material (i.e. LiCl) was utilised in the present work in order to promote nanoparticle formation and restricts the growth of large agglomerates of the desired

product phase. The removal of the salt by-product phase was also undertaken and changes regarding AlH_3 decomposition behaviour in washed samples were investigated.

2. Experimental

All handling of chemicals and sealable milling vials was undertaken in an argon-atmosphere glovebox in order to minimise oxygen ($O_2 < 5$ ppm) and water ($H_2O < 3$ ppm) contamination. All samples were analysed as close to synthesis as possible in order to prevent sample degradation, during storage, from affecting results. $LiAlH_4$ (Sigma-Aldrich, 95%), $AlCl_3$ (Sigma-Aldrich, 99%), and LiCl (Sigma-Aldrich, ≥99%) were used as starting reagents. Room temperature ball milling was performed with a custom made ball milling canister (650 cm^3 internal volume) attached to a Glen Mills Turbula T2C shaker mixer. The ball milling canister was made from stainless steel (316) and was sealed with an o-ring on both ends. The balls were made from the same material as the canister to minimise sample contamination due to the degradation of both the canister and balls. Cryogenic (77 K) milling was undertaken using a Spex 6850 freezer mill with both a supplied 190 cm^3 milling vial and a custom made [21] 14.3 cm^3 milling vial, using 145.5 g and 32 g milling rods respectively. Samples were milled with a LiCl buffer which was added to the initial reagents prior to milling to deter agglomeration and promote nanoparticle production. Milling parameters (such as ball size and milling time) were altered to explore the variety of reaction products.

The selection of an appropriate solvent is a crucial part of the synthesis process as the solvent must firstly be able to dissolve large quantities of the by-product phase (LiCl), it must be relatively unreactive to the alane nanoparticles, and it must also have a low viscosity so that it may be separated from the nanoparticles once it has dissolved the by-product phase. Solvent choice is made very difficult because alane is a powerful reducing agent and as such is very reactive with a range of solvents including a variety from the following groups: alcohols, phenols, amines, thiols, aldehydes, ketones, quinones, carboxylic acids, esters and lactones, epoxides, amides and nitriles, and some nitrogen and sulfur compounds [22]. Alane also dissolves in certain solvents which dissolve LiCl such as tetrahydrofuran (THF). However it has been found [22] that some nitro compounds and some sulfur compounds are relatively inert to alane. As such, nitromethane (Sigma-Aldrich, 96%) was used as the LiCl solvent. However in order to promote LiCl solubility in nitromethane, aluminium chloride was added

in a 3:1 ratio of $AlCl_3$:LiCl because the presence of certain other salts in solution have been found to promote the LiCl solubility in nitromethane [23].

Centrifugation was used to separate the solvent (containing the dissolved LiCl by-product phase) from the alane nanoparticle product, and the saline solution was decanted. Washing was performed three times, twice with a nitromethane/$AlCl_3$ mix and once with pure nitromethane. Room temperature milled AlH_3 samples did not present any visible signs of reaction with the solvent however noticeable gas evolution was present on addition of the cryogenically milled samples to the nitromethane/$AlCl_3$ solution. The gas evolution indicates an adverse reaction between the solvent and cryogenically milled sample. This is an indication that either the cryogenically milled alane is more reactive, or that a reaction between nitromethane and the $LiAlH_4$ starting reagent was observed due to the reaction of the cryogenically milled sample not reaching completion. It should be noted that $LiAlH_4$ is violently reactive with nitromethane and significant quantities of heat and fumes are generated upon contact with one another, even in dilute concentrations. Given the mild reaction between the solvent and the cryogenically milled sample it is unlikely that $LiAlH_4$ is present. As such a different solvent should be utilised in further studies in order to synthesise pure unreacted AlH_3 nanoparticles. Despite the observed reaction in cryogenically milled samples, the as-synthesised and washed alane samples were characterised to determine their hydrogen desorption kinetics and structural properties. The final washed alane product was put under vacuum for a few hours at room temperature to remove any final traces of solvent to obtain salt-free alane nanoparticles.

X-ray diffraction (XRD) was performed using a Siemens D500 diffractometer (CuK_α radiation) with a 2θ range of 10 - 80° using 0.02° steps with 3 s of count time per step with operating conditions of 40 kV and 30 mA. XRD was also undertaken on a Bruker D8 Advance diffractometer (CuK_α radiation) with a 2θ range of 10 - 100° using 0.02° steps with 0.8 s of count time per step with operating conditions of 40 kV and 40 mA. Samples were loaded into XRD sample holders in an argon glovebox and either sealed under a 4 μm mylar film or sealed within a poly(methylmethacrylate) (PMMA) air-tight holder to prevent oxygen/moisture contamination during data collection. The protective holders generate large amorphous humps in the data sets which were removed from the included figures for clarity via peak fitting in Topas (Bruker AXS, Karlsruhe, Germany). The background subtraction resulted in certain angular regions with increased noise content. Rietveld analysis was

performed on the XRD patterns using Topas in order to provide additional structural information from the crystalline phases in the washed and unwashed samples. The crystallite sizes were determined from an LVol-IB method (volume averaged column height calculated from the integral breadth) [24] which provides a good measure of the volume-weighted average crystallite size.

Transmission electron microscopy (TEM) was conducted on a JEOL JEM2011 instrument operating at 200 kV which was coupled with an Oxford Instruments energy dispersive x-ray spectrometer (EDS) for elemental analysis. Samples were loaded onto 200 mesh copper grids with holey carbon support films drop-wise via suspension in either nitromethane or toluene. The TEM grids contain minor traces of silicon resulting from the manufacturing process. Samples must be exposed to air before being loaded into the TEM column; however air-exposure time was kept as short as possible.

Hydrogen sorption experiments were performed in a manometric apparatus using the Hemmes equation of state [25] and the method of McLennan and Gray [26] to account for the compressibility of hydrogen. The digital pressure gauge (Rosemount 3051S) had a precision of 14 mbar and accuracy of 6 mbar, whilst room temperature measurements were recorded using a 4-wire platinum resistance temperature detector (RTD). Non-ambient sample temperatures were generated using a sealed tube furnace which was externally calibrated to ± 1°C.

3. Results and discussion

Aluminium hydride (AlH_3) has been reported to be stable in air for decades at room temperature due to its heavy oxide coating [9], however freshly mechanochemically synthesised alane is unstable due to its clean oxide-free surface, which does not significantly kinetically restrict decomposition. Alane is prone to decomposition as a result of its thermodynamic properties because ΔG of formation is positive at temperatures greater than approximately -200°C (when extrapolated from experimental data [27]). Theoretical calculations [28] suggest that ΔG of formation is positive (for the AlH_3 phases investigated) at all temperatures, and as such decomposition may occur spontaneously. Mechanochemically synthesised samples exhibit relatively rapid decomposition at room

temperature (significantly over months) when stored under an argon atmosphere. The decomposition is evidenced by XRD data provided in Figure 1, which displays a significant reduction in the AlH_3 content over one month, matched by an increase in the Al content of the sample when stored at ~ 25°C.

Quantitative phase analysis (QPA) results (see Table 1) outline the decomposition of the mechanochemically synthesised alane sample over time. After one month the alane content has been reduced to 73% of its as-synthesised content, increasing the aluminium content significantly. LiCl content does not change over time, although some $LiCl.H_2O$ is present in the aged sample due to an improper seal with the mylar film during data collection. The α'-AlH_3 phase decreased by 20.3% whereas the α-AlH_3 phase decreased by 31.9 % over one month.

The disproportionate decomposition indicates that α-AlH_3 decomposes more readily at room temperature, provided that α-AlH_3 does not undergo a phase transition to α'-AlH_3 during this time. The result is curious because α-AlH_3 is reported to be the most stable alane phase [9] as both β- and γ-AlH_3 were shown to transition to α-AlH_3 before decomposition evidenced by calorimetry [29] and in-situ XRD [30, 31]. The calorimetry results discount the possibility of an α-$AlH_3 \rightarrow \alpha'$-$AlH_3$ phase transition as no thermodynamic transitions were found during α-AlH_3 decomposition [29]. In fact, experimental and theoretical results [32] demonstrate that the opposite reaction can occur where α'-$AlH_3 \rightarrow \alpha$-AlH_3 if conditions are both kinetically and thermodynamically favourable. Therefore the disproportionate decomposition instead suggests a more rapid α-AlH_3 decomposition at room temperature in comparison to α'-AlH_3. In the literature α-AlH_3 is the phase which is synthesised reversibly via the reaction of hydrogen gas with aluminium at extreme pressures [12, 33]. The preferred formation may be due to α-AlH_3 having the most compact crystal structure, but the XRD results herein indicate that α'-AlH_3 is more stable over time at room temperature. In addition theoretical results also show [34] that α'-AlH_3 is more stable than α-AlH_3 in regards to the thermodynamics of decomposition. It is not know if the α'-AlH_3 stability (seen at room temperature herein) is a function of either kinetic or thermodynamic factors. The stability over time does not seem to be related to crystallite size as the average crystallite size of α-AlH_3 was found via Rietveld to be 15.0 ± 0.5 nm and 19 ± 1 nm for the 0 month and 1 month samples respectively whilst the average crystallite size was 17.0 ± 0.6 nm and 17 ± 1 nm for α'-AlH_3 in the 0 month and 1

month samples respectively. The crystallite sizes are comparable between both phases however it is possible that particle size differences between the phases could lead to different decomposition rates. It is also possible that any phase transformations to or from amorphous phases could bias these crystalline phase results obtained using QPA by the Rietveld method.

3.1. Room temperature synthesis

Room temperature mechanochemical synthesis is reported to produce low alane yields [3] due to the decomposition of AlH_3 to Al and H_2 resulting from the energy provided during milling. Room temperature ball milling was undertaken under a variety of milling conditions in order to understand the impact of these conditions on AlH_3 yields and phase production. Initially room temperature milling was undertaken using a mixture of 12.7 mm & 7.938 mm balls with a 39:1 ball to powder ratio (B:P) and a LiCl buffer was used to provide a 2.2:1 volume ratio of $LiCl:AlH_3$ in the final product. However it was determined via XRD that more than 50% of the synthesised AlH_3 had decomposed to Al during just one hour of milling. The rapid decomposition is a result of the significant energy provided during milling from the large balls. As a result room temperature milling was undertaken using 4 mm balls in a smaller 13:1 B:P ratio in order to lower the milling energy and reduce the decomposition of the as-synthesised AlH_3. XRD was undertaken after milling for 2, 4, and 6 hours as provided in Figure 2.

QPA results (see Table 2) outline the crystalline sample composition as a function of milling time. Crystalline α'-AlH_3 is present in moderate quantities in the sample milled for 2 hours (Figure 2A), however the alane content is reduced almost to zero in samples which were milled for longer (Figure 2B & 2C). Minor trace phases of both β-AlH_3 and γ-AlH_3 are noted in some XRD patterns (Figure 2A & 2B), which indicate that alane phase transformations are occurring during milling. Despite the very low crystalline AlH_3 content in the 6 hour milled sample, given by XRD (Figure 2C), hydrogen sorption measurements indicate that the sample contains a considerable portion of AlH_3. The 6 hour as-milled sample was incrementally ramped to 150°C over 120 hours and desorbed a quantity of hydrogen that equates to a 8.1 wt.% AlH_3 content in the entire synthesised sample (from a theoretical maximum of 24.6 wt.%). This desorption result in conjunction with the decline in crystalline Al and AlH_3 content with increasing milling time indicates that there is non-crystalline Al and AlH_3

present in the sample after milling at room temperature with small 4 mm balls. It may also be possible that the as-synthesised AlH_3 is so nanoscopic that some XRD peaks are hidden under the background noise. To the authors' knowledge non-crystalline AlH_3 has not been previously reported in the literature. Theoretical investigations have suggested the possibility of crystalline AlH_3 phases existing in real samples which have not been identified experimentally to date [28]. However, given that no unidentified crystalline peaks are present in the XRD patterns it is unlikely that these phases exist in the samples herein.

TEM investigations of the room temperature synthesised alane nanoparticles were performed whilst they were still embedded in salt and after they had been washed with nitromethane & $AlCl_3$ (to remove the LiCl by-product phase). The micrograph provided in Figure 3A illustrates alane nanoparticles (~ 100 nm) embedded within larger (~ 400 nm) salt clusters. It can be seen in Figure 3B that the alane nanoparticles decompose under the electron beam after a short time (2 min) resulting in a decrease in particle size. After samples were washed (removing LiCl) two distinct particle morphologies existed: Large geometric-shaped single crystals as shown in Figure 3C and clusters of small irregularly shaped crystals as shown in Figure 3D. The large crystal in Figure 3C was identified as a LiCl single crystal via electron diffraction. Given that the LiCl phase is not detectable using lab-based XRD, its presence only in TEM investigations suggests that it is a minor sample component that is a remnant from the washing process. The washed sample primarily consisted of the smaller crystals shown in Figure 3D, which were identified as Al-rich via energy dispersive x-ray spectroscopy (EDS) during TEM investigations, indicating that these crystals are either AlH_3 or Al (resulting from alane decomposition). The washed AlH_3/Al nanoparticles in Figure 3D are aggregated together but consist of $30 - 50$ nm particles which appear similar to TEM micrographs of dehydrided α-AlH_3 particles recently presented in the literature [35], although those herein seem to be clusters of separate particles rather than large particles with internal structure.

3.2. Cryogenic synthesis

Cryogenic (77 K) milling provides high alane yields (low Al content) due to the low milling temperatures, which minimises the decomposition of alane in contrast to room temperature milling [3]. XRD was utilised to analyse samples that were cryogenically milled for increasing times without the use of a reaction buffer material as shown in Figure 4. XRD data

after milling for 1 minute (not included here) indicates only starting reagents ($AlCl_3$, $LiAlH_4$, and $LiCl$) are present. For samples milled for 15 minutes or longer no starting reagents are detected and AlH_3 and $LiCl$ are the only crystalline phases present. The XRD data shows that samples milled for 15 and 30 minutes have both α'-AlH_3 and α-AlH_3 phases in similar ratios, however for the sample milled for 60 min the α-AlH_3 phase is dominant. QPA results indicate that the Al wt.% is 3.0, 5.0, and 11.9 ± 0.3 for the 15, 30, and 60 min samples respectively. Thus longer milling times result in higher Al yields due to the longer times in which AlH_3 is exposed to high energy milling. However the Al content in cryogenically synthesised samples is much lower than those measured in room temperature synthesised samples, indicating that the low milling temperatures do restrict AlH_3 decomposition and prevent high Al yields.

In order to promote nanoparticle formation, samples were cryogenically milled for 60 minutes with a large quantity of reaction buffer (2:1 $LiCl$:AlH_3 volume ratio). XRD results are provided in Figure 5A for the as-milled sample, which show a high α-AlH_3 yield with minor α'-AlH_3 and Al phases as well as the $LiCl$ reaction by-product phase. The result is similar to the reaction undertaken cryogenically with no reaction buffer where high α-AlH_3 yields are encountered with some Al decomposition product present. A sample of as-milled powder was washed using nitromethane and $AlCl_3$ to remove the $LiCl$ by-product phase. However noticeable gas evolution was apparent upon addition of the sample to the nitromethane/$AlCl_3$ solution during washing indicating that a reaction between the AlH_3 and the solution occurred. Gas evolution was not noticeable when washing mechanochemically synthesised pure Al nanoparticles [36] indicating that cryogenically synthesised alane is much more reactive than Al even though gas evolution from alane would be more noticeable due to its internal hydrogen supply. Even though a reaction with the solvent was noted, XRD of the washed sample as shown in Figure 5B does not show any unwanted crystalline reaction products. The only crystalline phases present in the washed sample are α'-AlH_3, α-AlH_3, and Al.

Hydrogen desorption experiments were undertaken within 1 week of sample synthesis and/or washing to ensure room temperature alane decomposition was minimised. Both unwashed (as-milled) and washed samples of cryogenically synthesised alane (2:1 $LiCl$:AlH_3 volume ratio) were loaded into a manometric hydrogen sorption apparatus and initially evacuated at room temperature for 30 minutes. The samples were then raised to 50°C and held at this

temperature for 24 hours, followed by 24 hours at 100°C and then 150°C respectively in order to examine the kinetic behaviour and maximum desorbed wt.% of the samples. Hydrogen desorption data is displayed in Figure 6 which depicts the wt.% of H_2 as a function of time in the calculated non-salt portions of the unwashed and washed samples. This relates to the percentage of hydrogen desorbed from the Al/AlH$_3$ portions of the samples (26.43% and 100% of the unwashed and washed samples respectively).

Alane is thermodynamically unstable over a large temperature range and its decomposition is in fact only kinetically limited. Kinetic barriers are crucial in stabilising alane at moderate temperatures given its extreme equilibrium pressures (i.e. 28 kbar at 300°C [11, 12]). The unwashed sample desorbs a significant quantity of hydrogen (3 wt.% H_2 from Al) over 24 hours at 50°C. This indicates rapid decomposition at a lower temperature than results reported for bulk, Dow-synthesised alane which provide adequate kinetics often in the order of 100°C, although these kinetics can be enhanced by doping [9]. However similar kinetics to those reported herein have been observed for freshly synthesised alane decomposed at 60°C [7]. Figure 6 shows that rapid desorption occurs at 100°C and raising the sample temperature to 150°C results in complete hydrogen desorption. The resultant measured alane content is 25.0 wt.% in the total sample with only a calculated as-milled 1.4 wt.% Al content (73.6% LiCl). The desorption kinetics will likely be hindered by the fact that the alane particles are embedded within a LiCl salt matrix. Restricted desorption kinetics are beneficial during room temperature storage but LiCl is not fully effective in kinetically stabilising alane decomposition.

The hydrogen desorption results for the washed alane sample are interesting. Firstly desorption kinetics are significantly slower, and secondly the maximum H_2 wt.% is half that of the unwashed sample. Desorption kinetics should be quicker for the washed sample due to the absence of kinetically hindering LiCl salt. However, the slower observed kinetics suggest a limiting factor may be present. Aluminium oxide surface layers can be detrimental to molecular [37] and even atomic [38] hydrogen permeation. Despite XRD showing only AlH$_3$ and Al in the washed samples, the evolution of gas upon addition of the as-synthesised sample to nitromethane suggests that an unwanted (oxide/hydroxide) phase may have formed. The formation of amorphous aluminium oxide phases rather than crystalline phases have been theoretically shown to be thermodynamically favourable [39]. The theoretical results in

the literature have also been reinforced by experimental amorphous oxide formation [40]. Given that no oxide or hydroxide phases were detected with XRD and that the maximum H_2 wt.% is half that of the unwashed sample it seems likely that the washed sample contains a significant amorphous aluminium oxide/hydroxide phase. The extent of oxide contamination would be exacerbated by the small particle size of the synthesised AlH_3 nanoparticles that provides a large surface area in which oxide formation can occur.

XRD was also performed on the desorbed unwashed and washed alane samples (see Figure 7). The XRD data verifies that hydrogen desorption was complete for both samples. No crystalline oxide or hydroxide phases are observed in the desorbed sample XRD patterns which were taken after sample heating to 150°C. QPA results provided in Table 3 display the crystalline compositions of both the unwashed and washed alane samples before and after desorption. A comparison between the AlH_3 content derived from hydrogen desorption measurements for the unwashed sample (25.0 wt.%) and the AlH_3 content from XRD results (15.8 wt.%) reveals a disparity between the total amount of alane in the sample and the crystalline content. These results suggest that at least 37% of the alane present in the unwashed sample is non-crystalline.

Based on knowledge of the sample history and crystallite size trends (see Table 3), information regarding alane crystallite behaviour upon washing and desorption can be gained. A comparison between unwashed and washed samples reveals an increase in the average crystallite size of AlH_3 and Al upon washing. An average crystallite size increase may occur from two phenomena. Firstly, centrifugation preferentially separates the largest AlH_3/Al particles from solution first, and it is possible that the smallest particles remained in solution increasing the average separated crystallite size. Secondly, it is possible that exothermic amorphous oxide formation during the washing procedure generated heat that promoted crystallite growth in solution. Alternatively physical contact between AlH_3/Al particles upon the removal of the salt matrix may have also resulted in particle agglomeration and crystallite growth.

A comparison between the XRD data for desorbed samples and their precursor materials also reveals alane crystallite behaviour. In the unwashed samples it appears that the 2:1 volume ratio between LiCl and AlH_3 may be insufficient to completely separate the AlH_3 particles.

Previous research [41] has required using volume ratios as high as 10:1 to result in well separated particles. Consequently, during desorption (heating to 150°C), crystallite size may increase due to both intra-particle crystallite growth and inter-particle agglomeration. In the washed samples, there is very little difference in the crystallite size of the Al upon heating to 150°C. Intra-particle crystallite growth may have already occurred during the washing process and the amorphous oxide coating generated during this washing may hinder inter-particle growth during heating.

4. Conclusions

Alane nanoparticles have been synthesised via both room temperature and cryogenic mechanochemical synthesis. The evolution of alane production was investigated as a function of milling time under a variety of milling conditions. Cryogenic milling was verified to form higher yields of AlH_3 and four different crystalline alane phases (α, α', β, γ) were identified via XRD structural investigations. The LiCl reaction by-product phase was removed via washing with a nitromethane/$AlCl_3$ solution, which adversely reacted with the AlH_3 nanoparticles. The hydrogen desorption kinetics for the washed sample were hindered and the maximum H_2 wt.% was halved, although no crystalline oxide or hydroxide phases were found via XRD. Unwashed mechanochemically synthesised AlH_3 was found to desorb at room temperature over months and significantly at 50°C in a 24 hour period. QPA results coupled with hydrogen desorption measurements suggest the presence of an amorphous AlH_3 phase in mechanochemically synthesised samples, which deserves further study to identify its structural characteristics. If mechanochemically synthesised alane is to be successfully washed from LiCl a less reactive solvent must be discovered which will not alter the alane particle surface. However, alane without a kinetic barrier to hydrogen desorption is extremely unstable at room temperature.

References

[1] A.E. Finholt, A.C. Bond Jr., H.I. Schlesinger, J. Am. Chem. Soc. 69 (1947) 1199-1203.
[2] M.A. Petrie, J.C. Bottaro, R.J. Schmitt, P.E. Penwell, D.C. Bomberger, *US Patent* 6,228,338 B1, 8 May, 2001.
[3] H.W. Brinks, A. Istad-Lem, B.C. Hauback, J. Phys. Chem. B 110 (2006) 25833-25837.
[4] H.W. Brinks, W. Langley, C.M. Jensen, J. Graetz, J.J. Reilly, B.C. Hauback, J. Alloys Compd. 433 (2007) 180-183.
[5] H.W. Brinks, C. Brown, C.M. Jensen, J. Graetz, J.J. Reilly, B.C. Hauback, J. Alloys Compd. 441 (2007) 364-367.
[6] F.M. Brower, N.E. Matzek, P.F. Reigler, H.W. Rinn, C.B. Roberts, D.L. Schmidt, J.A. Snover, K. Terada, J. Am. Chem. Soc. 98 (1976) 2450-2453.
[7] J. Graetz, J.J. Reilly, J. Phys. Chem. B 109 (2005) 22181-22185.
[8] J. Graetz, J.J. Reilly, J.G. Kulleck, R.C. Bowman, J. Alloys Compd. 446-447 (2007) 271-275.
[9] G. Sandrock, J. Reilly, J. Graetz, W.-M. Zhou, J. Johnson, J. Wegrzyn, Appl. Phys. A 80 (2005) 687-690.
[10] G. Sandrock, J. Reilly, J. Graetz, W.-M. Zhou, J. Johnson, J. Wegrzyn, J. Alloys Compd. 421 (2006) 185-189.
[11] B. Baranowski, M. Tkacz, Z. Phys. Chem. 135 (1983) 27-38.
[12] S.K. Konovalov, B.M. Bulychev, Inorg. Chem. 34 (1995) 172-175.
[13] R. Zidan, B.L. Garcia-Diaz, C.S. Fewox, A.C. Stowe, J.R. Gray, A.G. Harter, Chem. Comm. (2009) 3717-3719.
[14] G.S. McGrady, *US Patent* US 2008/0241056 A1, 2 October, 2008.
[15] J. Graetz, Chem. Soc. Rev. 38 (2009) 73-82.
[16] J. Ding, T. Tsuzuki, P.G. McCormick, R. Street, J. Alloys Compd. 234 (1996) L1-L3.
[17] P.G. McCormick, T. Tsuzuki, J.S. Robinson, J. Ding, Adv. Mater. 13 (2001) 1008-1010.
[18] P.G. McCormick, J. Ding, W.-F. Miao, R. Street, *US Patent* 6,203,768 B1, 20 March, 2001.
[19] T. Tsuzuki, P.G. McCormick, J. Mater. Sci. 39 (2004) 5143-5146.
[20] C. Suryanarayana, Prog. Mater. Sci. 46 (2001) 1-184.
[21] Personal communication: E.MacA. Gray, M.P. Pitt., Griffith University, Australia.
[22] H.C. Brown, N.M. Yoon, J. Am. Chem. Soc. 88 (1966) 1464-1472.
[23] H.V.A. Briscoe, A.A. Eldridge, G.M. Dyson, A.J.E. Welch (Eds.), Mellor's Comprehensive Treatise on Inorganic and Theoretical Chemistry, Longman Group Limited, London, 1972.
[24] A.A. Coelho, Topas User Manual, Bruker AXS GmbH, Karlsruhe, Germany, 2003.
[25] H. Hemmes, A. Driessen, R. Griessen, J. Phys. C: Solid State Phys. 19 (1986) 3571-3585.
[26] K.G. McLennan, E.MacA. Gray, Meas. Sci. Technol. 15 (2004) 211-215.
[27] Outukumpu, HSC Chemistry 6.1, Chemistry Software, Houston, 2006.
[28] S. Sun, X. Ke, C. Chen, I. Tanaka, Phys. Rev. B 79 (2009) 024104.
[29] J. Graetz, J. Reilly, J. Alloys Compd. 424 (2006) 262-265.
[30] H. Grove, M.H. Sørby, H.W. Brinks, B.C. Hauback, J. Phys. Chem. C 111 (2007) 16693-16699.

[31] J.P. Maehlen, V.A. Yartys, R.V. Denys, M. Fichtner, Ch. Frommen, B.M. Bulychev, P. Pattison, H. Emerich, Y.E. Filinchuk, D. Chernyshov, J. Alloys Compd. 446-447 (2007) 280-289.

[32] S. Sartori, S.M. Opalka, O.M. Løvvik, M.N. Guzik, X. Tang, B.C. Hauback, J. Mater. Chem. 18 (2008) 2361-2370.

[33] H. Saitoh, A. Machida, Y. Katayama, K. Aoki, Appl. Phys. Lett. 93 (2008) 151918.

[34] X. Ke, A. Kuwabara, I. Tanaka, Phys. Rev. B 71 (2005) 184107.

[35] K. Ikeda, S. Muto, K. Tatsumi, M. Menjo, S. Kato, M. Bielmann, A. Züttel, C.M. Jensen, S. Orimo, Nanotechnol. 20 (2009) 204004.

[36] M. Paskevicius, J. Webb, M.P. Pitt, T.P. Blach, B.C. Hauback, E.MacA. Gray, C.E. Buckley, J. Alloys Compd. 481 (2009) 595-599.

[37] J.L. Maienschein, R.G. Musket, F.E. McMurphy, D.W. Brown, Appl. Phys. Lett. 50 (1987) 940-942.

[38] Y. Yamada-Takamura, F. Koch, H. Maier, H. Bolt, Surf. Coat. Technol. 153 (2002) 114-118.

[39] L.P.H. Jeurgens, W.G. Sloof, F.D. Tichelaar, E.J. Mittemeijer, Phys. Rev. B 62 (2000) 4707-4719.

[40] L.P.H. Jeurgens, W.G. Sloof, F.D. Tichelaar, E.J. Mittemeijer, J. Appl. Phys. 92 (2002) 1649-1656.

[41] T. Tsuzuki, J. Ding, P.G. McCormick, Physica B 239 (1997) 378-387.

Tables and Figures

Table 1: Crystalline QPA results from Rietveld fits to XRD data given in Figure 1. Mathematical fitting uncertainties of one standard deviation are provided.

	Phase	Crystalline wt. %	Crystallite size (nm)
0 Month	α'-AlH3	14.8 ± 0.2	16.1 ± 0.6
	α-AlH3	19.1 ± 0.3	15.0 ± 0.4
	Al	3.6 ± 0.1	18.0 ± 1.2
	LiCl	62.5 ± 0.3	27.5 ± 1.0
1 Month	α'-AlH3	11.8 ± 0.3	15.6 ± 1.0
	α-AlH3	13.0 ± 0.3	23.8 ± 1.2
	Al	13.4 ± 0.2	30.0 ± 0.9
	LiCl	59.4 ± 0.4	25.4 ± 1.0
	LiCl.H2O	2.3 ± 0.2	18.8 ± 10.2

Table 2: Crystalline QPA results from Rietveld fits for the 2, 4, and 6 hour room temperature milled sample XRD patterns given in Figure 2. Mathematical fitting uncertainties of one standard deviation are provided. Some crystallite sizes are not included due to the very low phase wt.% which makes results unreliable.

	Phase	Crystalline wt. %	Crystallite size (nm)
2 hour	α'-AlH$_3$	12.0 ± 0.1	36.9 ± 1.6
	β-AlH$_3$	0.7 ± 0.1	-
	Al	3.7 ± 0.1	64.6 ± 4.3
	LiCl	81.7 ± 0.3	407.4 ± 83.6
	LiAlH$_4$	1.9 ± 0.3	-
4 hour	α'-AlH$_3$	0.7 ± 0.1	-
	γ-AlH$_3$	2.6 ± 0.2	58.7 ± 16.5
	Al	2.2 ± 0.1	71.5 ± 9.9
	LiCl	92.0 ± 0.4	130.0 ± 10.6
	LiAlH$_4$	2.4 ± 0.4	-
6 hour	α'-AlH$_3$	0.4 ± 0.1	-
	Al	2.0 ± 0.1	43.2 ± 5.2
	LiCl	97.5 ± 0.1	65.3 ± 3.2

Table 3: Crystalline QPA results from Rietveld fits for XRD patterns given in Figure 5 and 7 for unwashed and washed alane samples before and after desorption. Wt.%, crystallite sizes, and mathematical fitting uncertainties of one standard deviation are provided.

	Phase	Crystalline wt. %	Crystallite size (nm)
Unwashed	α'-AlH$_3$	5.8 ± 0.4	11.3 ± 1.7
	α-AlH$_3$	10.0 ± 0.3	20.5 ± 1.0
	Al	2.7 ± 0.3	7.9 ± 1.3
	LiCl	81.5 ± 0.5	40.5 ± 1.8

Unwashed – Desorbed	Al	23.9 ± 0.1	39.0 ± 0.6
	LiCl	76.1 ± 0.1	81.0 ± 3.1
Washed	α'-AlH$_3$	28.4 ± 0.2	17.7 ± 0.3
	α-AlH$_3$	62.9 ± 0.2	21.5 ± 0.2
	Al	8.8 ± 0.1	22.3 ± 0.7
Washed – Desorbed	Al	100	26.1 ± 0.1

Figure 1: X-ray Diffraction (XRD) patterns from mechanochemically synthesised alane undertaken cryogenically (77 K) with no buffer, which is shown to decompose significantly over time. The patterns are background subtracted for clarity. Rietveld fits to the data are also displayed (solid line) along with difference plots.
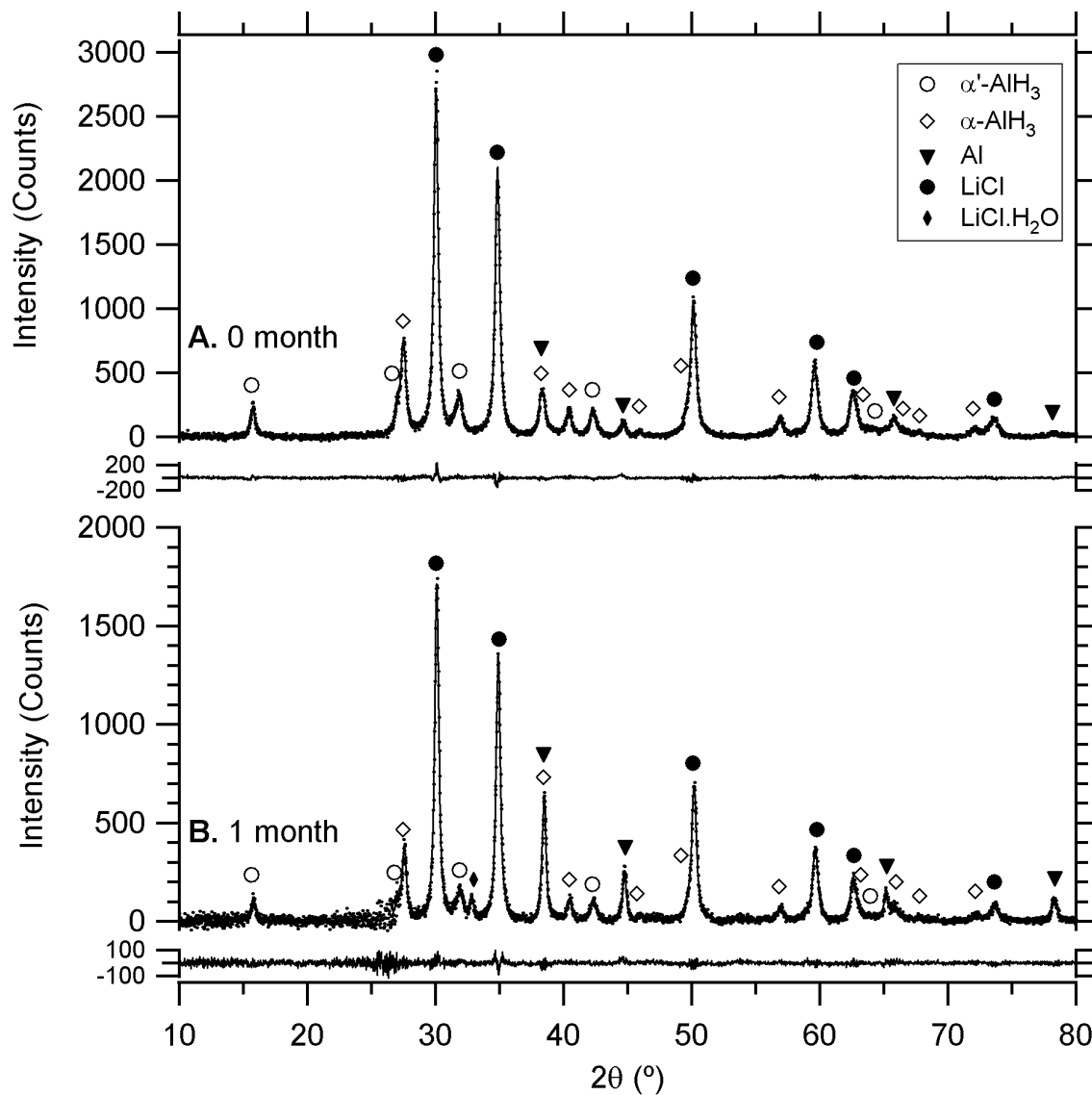
Figure 2: X-ray diffraction patterns from mechanochemically synthesised alane undertaken at room temperature with a 2.2:1 LiCl:AlH$_3$ volume ratio for A) 2 hours, B) 4 hours, & C) 6 hours. The patterns are mylar subtracted, offset and the square root of intensity is displayed for clarity, however a high-noise region exists due to the subtraction of a large mylar hump. Rietveld fits to the data are also displayed (solid line) along with difference plots.
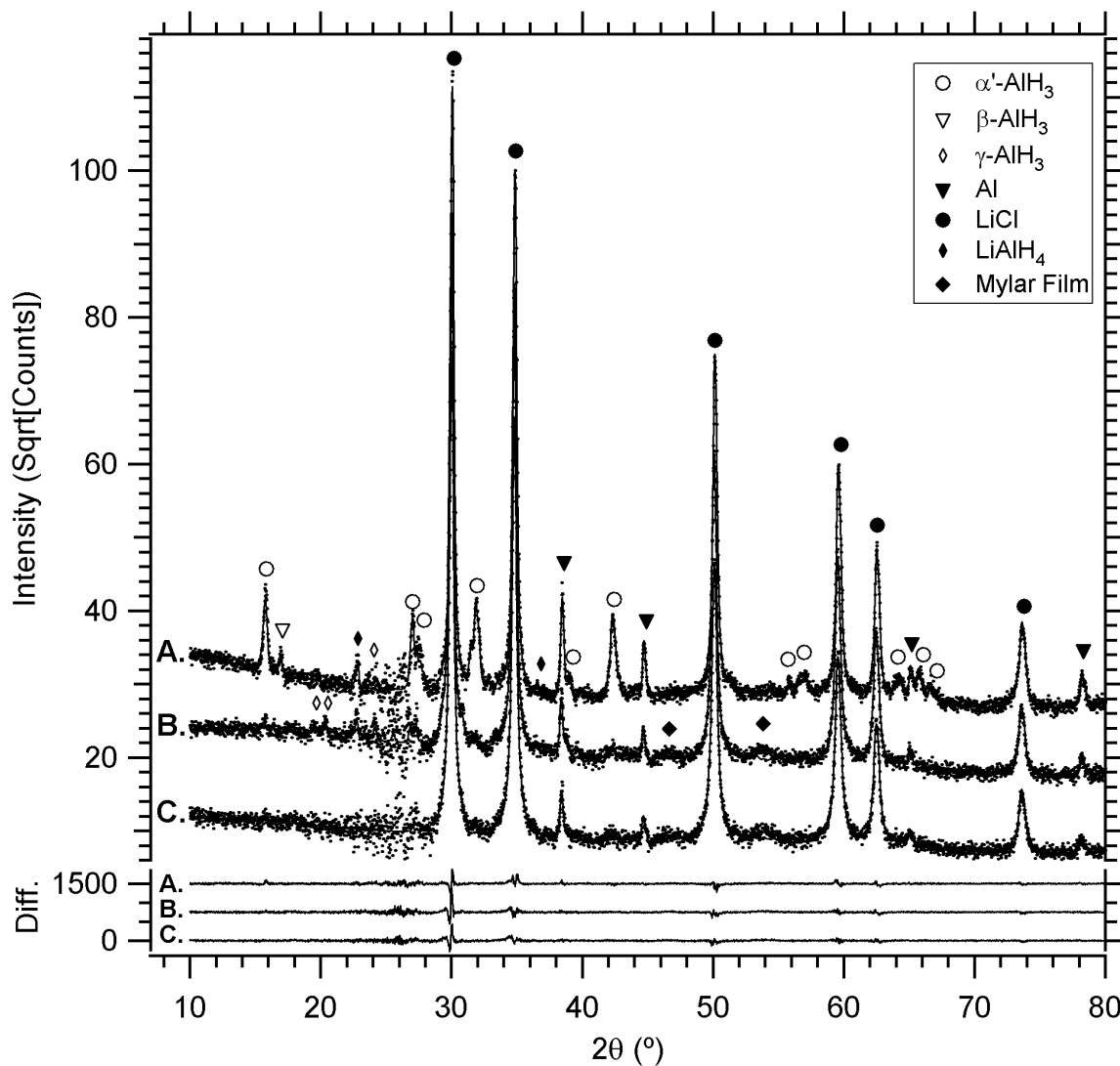
Figure 3: TEM micrographs of as-milled samples which display A) AlH_3 nanoparticles embedded in a larger LiCl salt cluster initially and B) after 2 minutes under the beam. Washed samples show C) low quantities of LiCl crystals and predominantly D) small $30 - 50$ nm Al/AlH_3 particles in aggregate clusters. White arrows depict the AlH_3 particle which decreased in size over time.

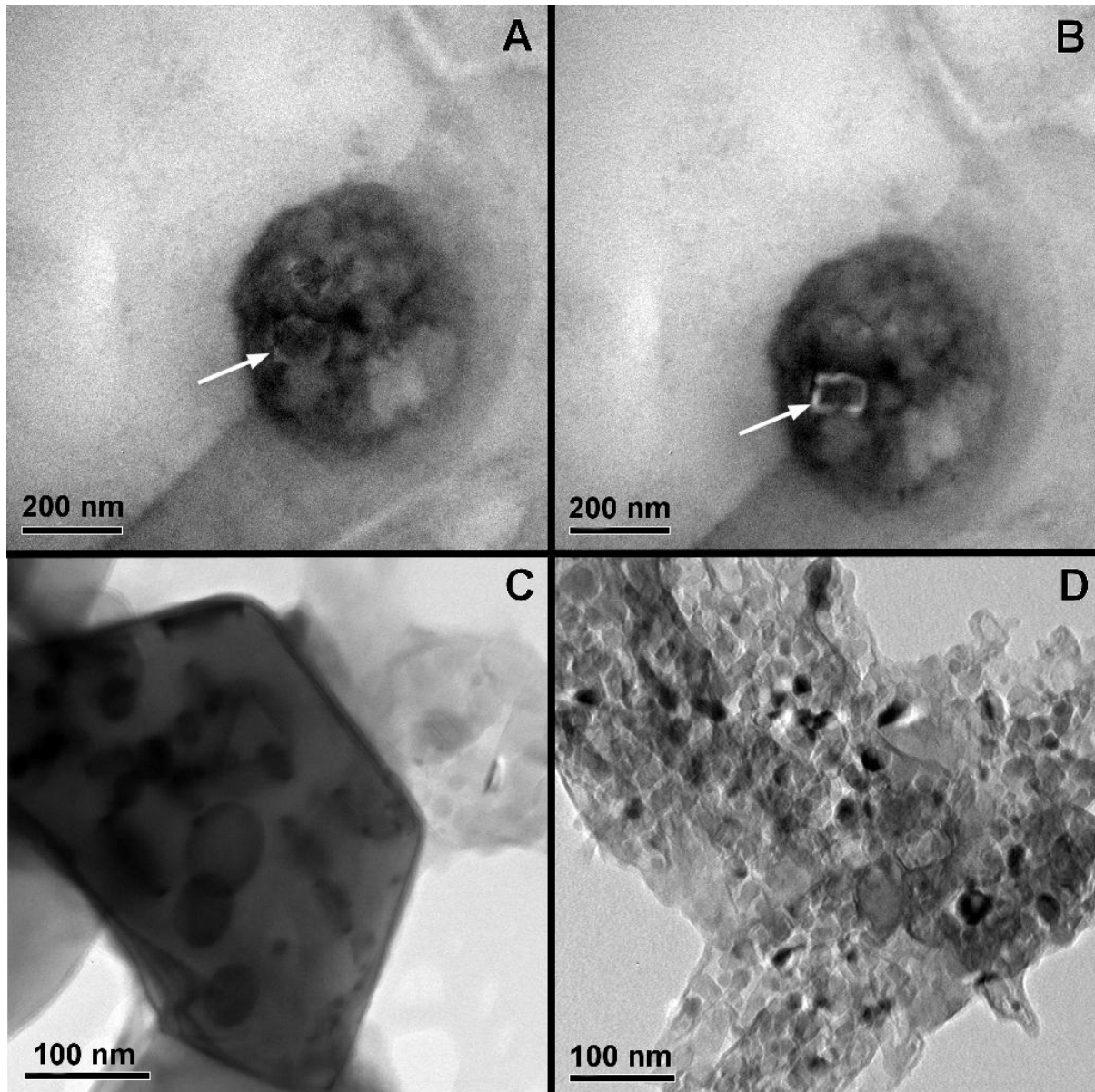Figure 4: X-Ray Diffraction (XRD) patterns from mechanochemically synthesised alane undertaken cryogenically with a 0.76:1 LiCl:AlH$_3$ final volume ratio, which were milled for A) 15 minutes B) 30 minutes and C) 60 minutes. Patterns have been background subtracted and offset for clarity. Rietveld fits to the data are also displayed (solid line) along with difference plots.
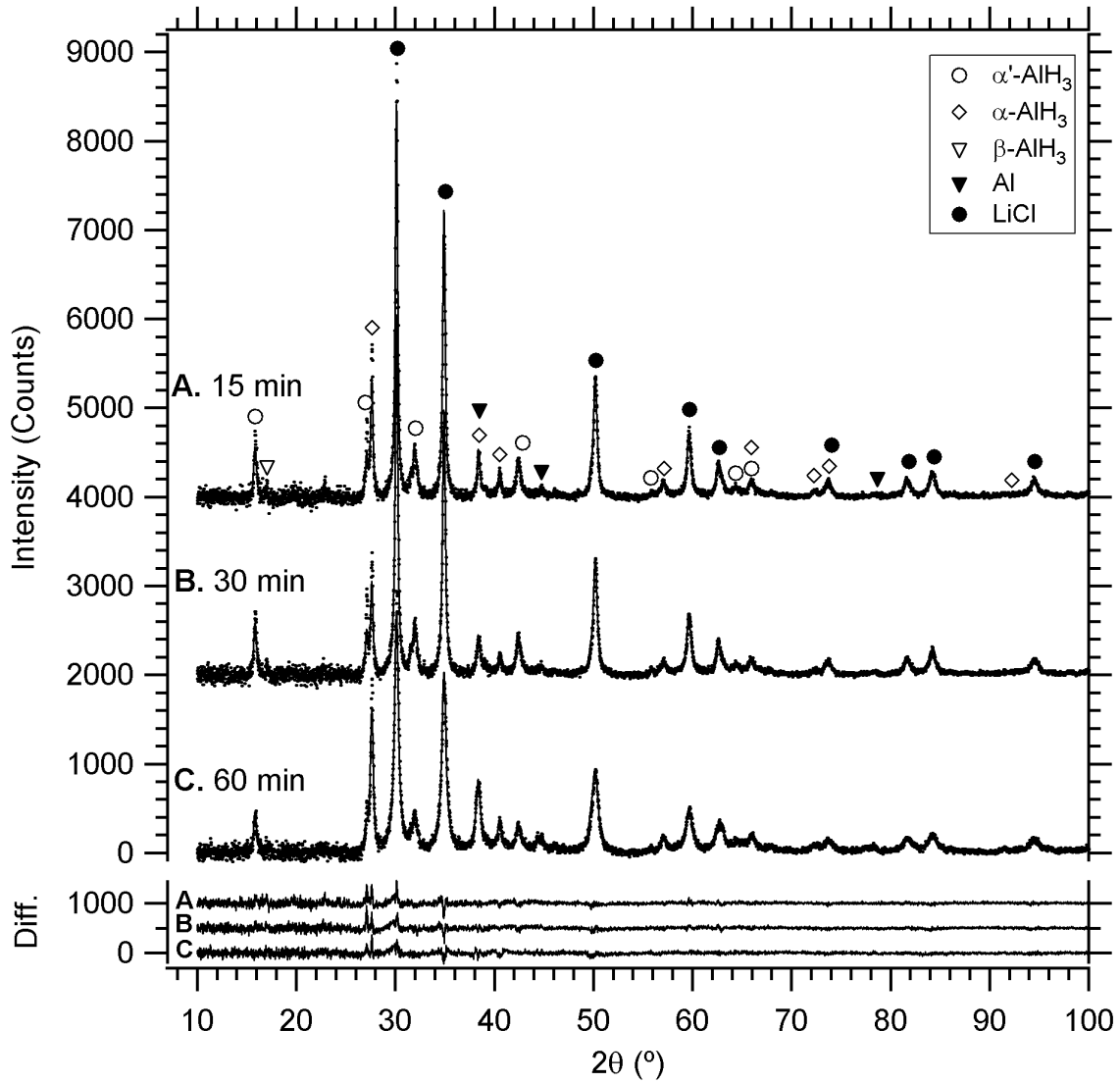
Figure 5: X-Ray Diffraction (XRD) patterns for cryogenically synthesised alane milled for 1 hour with a 2:1 LiCl:AlH$_3$ volume ratio A) before and B) after washing with nitromethane & AlCl$_3$. Patterns have been background subtracted for clarity. Rietveld fits to the data are also displayed (solid line) along with difference plots.
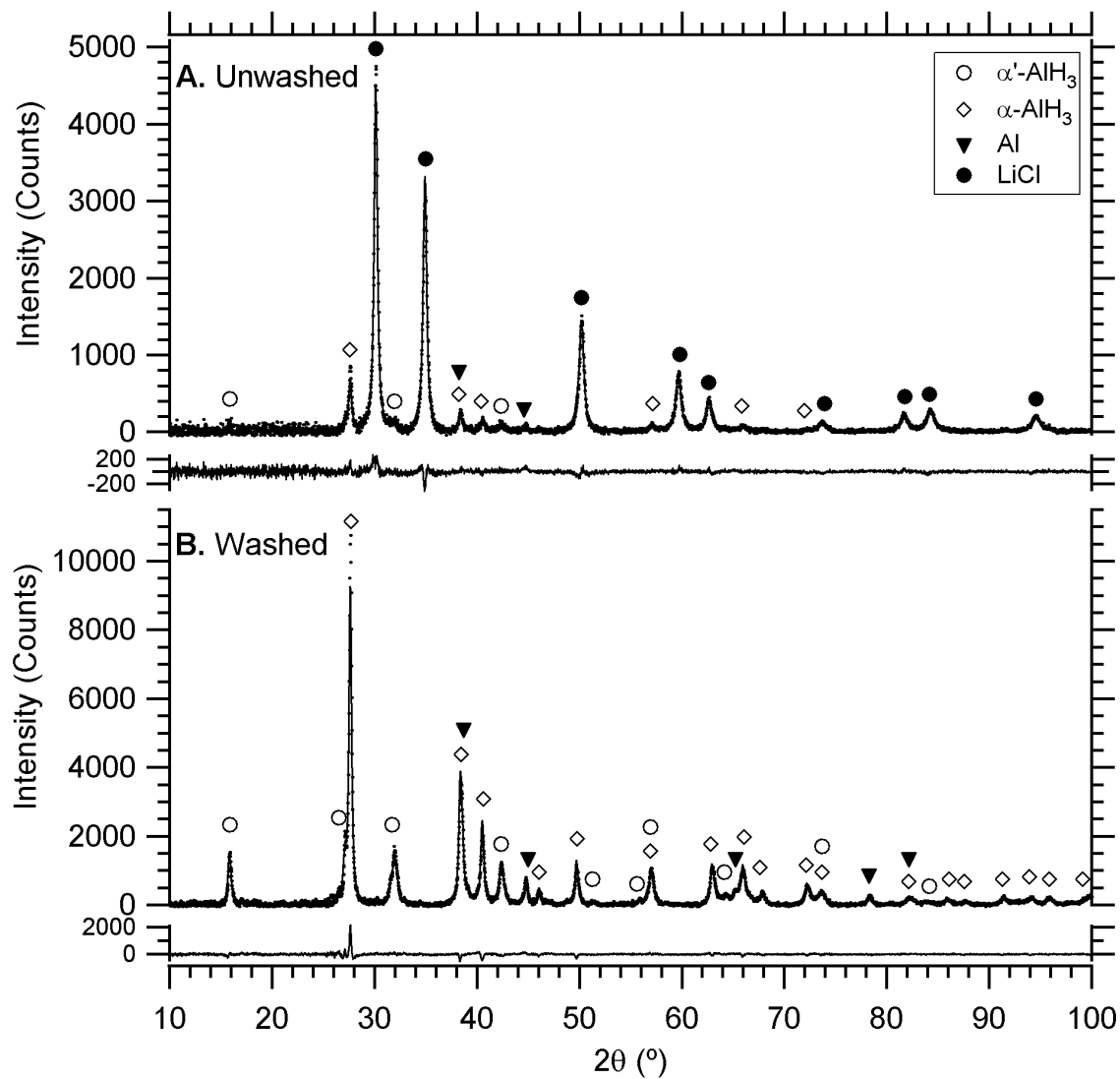
Figure 6: Hydrogen desorption data from A) unwashed and B) washed samples cryogenically milled for 1 hour with a 2:1 LiCl:AlH$_3$ volume ratio. The H$_2$ wt.% is given as a percentage of the calculated non-salt portion of the samples. Data was collected every 2 min for 24 hour periods at each temperature consecutively.
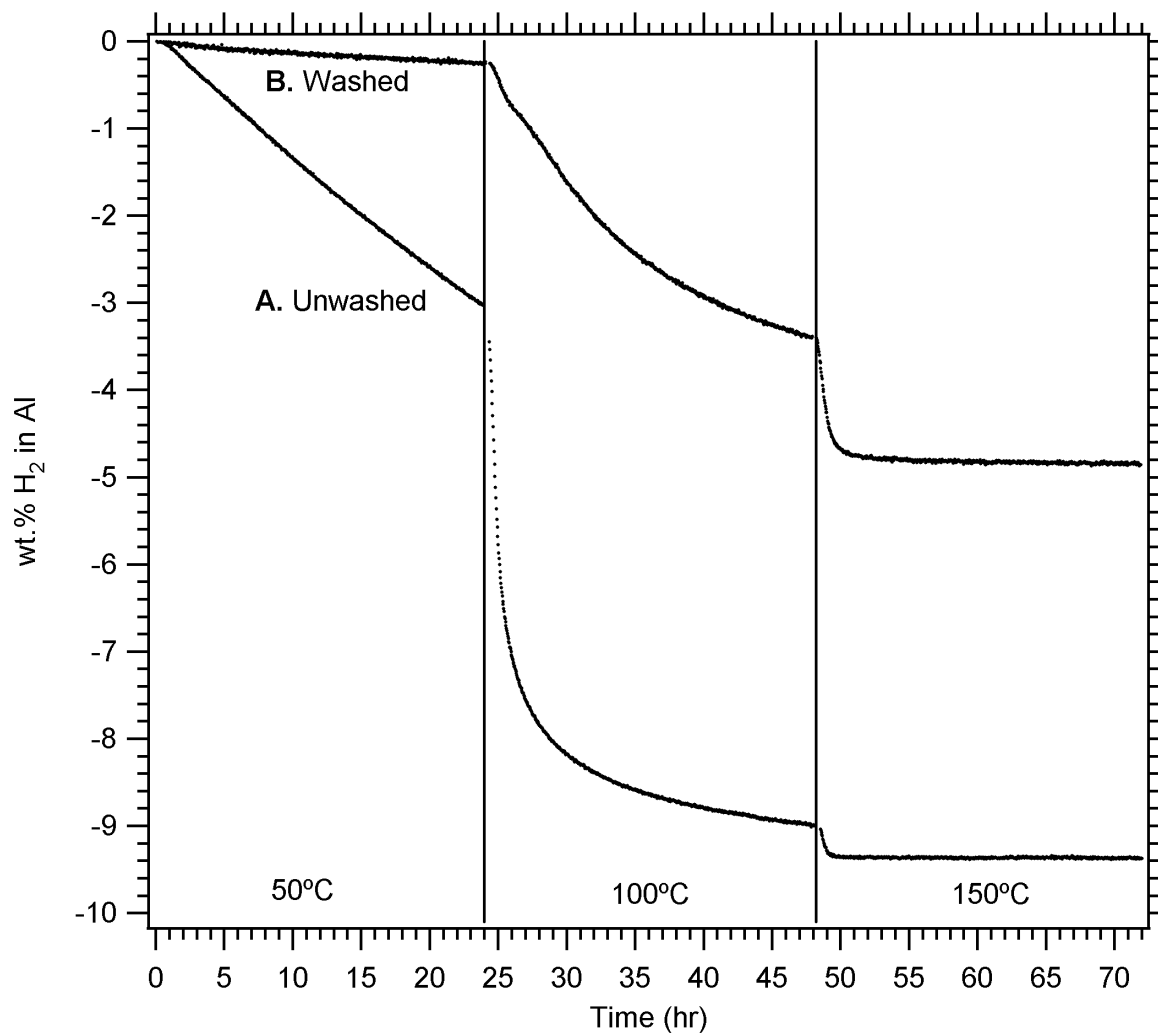
Figure 7: X-Ray Diffraction (XRD) patterns for desorbed cryogenically synthesised alane milled for 60 min with a 2:1 LiCl:AlH_3 volume ratio A) before and B) after washing with nitromethane & $AlCl_3$. Patterns have been background subtracted for clarity. Rietveld fits to the data are also displayed (solid line) along with difference plots.